Journal of Radioanalytical and Nuclear Chemistry (2023) 332:3235–3247
https://doi.org/10.1007/s10967-023-08976-4

Bio-waste derived hydroxyapatite nano rods for U(VI) uptake from aqueous medium

A. Dhanasekaran[1] · G. Suresh[2] · Ilaiyaraja Perumal[1] · N. Priyadarshini[3] · K. Dhanaraj[4] · R. M. Vimalathithan[5]

Received: 31 March 2023 / Accepted: 21 May 2023 / Published online: 5 June 2023
© Akadémiai Kiadó, Budapest, Hungary 2023

Abstract

Hydroxyapatite Nano Rods (HAp-NR) was synthesized from *Perna viridis* shell bio-waste by chemical precipitation method followed by annealing with addition of poly vinyl alcohol (PVA). The formation of HAp-NR was confirmed by FTIR and XRD analysis. SEM and TEM images confirms rod like structure of HAp and the EDX studies have confirmed the presence of Ca, P and O with Ca/P ratio = 1.61 in HAp-NR. Removal of uranium (VI) from aqueous solution by batch adsorption experiments was investigated using HAp-NR. The influence of pH, contact time, initial U(VI) concentration, temperature and ionic strength on adsorption of U(VI) onto HAp-NR were carried out. The adsorption of U(VI) onto HAp-NR was confirmed by EDS elemental mapping, FTIR, and XRD studies. Kinetics of adsorption followed the Elovich model and the adsorption process reached equilibrium within 90 min. Adsorption isotherm data agreed well with the Langmuir isotherm model and HAp-NR exhibits maximum experimental adsorption capacity of 293.6 mg g^{-1} at 298 K. Temperature dependent adsorption studies reveals the endothermic nature of U(VI) adsorption onto HAp-NR. The adsorbent can be reused by leaching the adsorbed U(VI) by equilibrating with 0.05 M Na_2CO_3. Hence, the present study reveals that HAp-NR derived from *Perna viridis* shell bio-waste could be a potential simplistic nanomaterial for environmental remediation.

Keywords Nanohydroxyapatite · Biowaste · Chemical precipitation · Uranium · Sea shell

Introduction

Humans rely on the maritime environment for a variety of economic reasons, including the supply of food, medicine, and various raw materials. In the recent years, marine-derived biomolecules (proteins, natural compounds, etc.) are gaining wide attention in medicine and engineering fields. Marine environments are home to many exotic biological species that may inspire the designing of biomimetic materials such as bioceramics [1]. Hydroxyapatite (HAp), one of the bioactive ceramics has gained wide attention in recent years due to its potential applications in several fields such as bioceramic industry, medical, pharmaceutical, and also in the environmental pollution control [2].

HAp is chemically represented as $Ca_{10}(PO_4)_6(OH)_2$. It can be obtained from both chemical and natural sources [3–7]. The Ca/P ratio of stoichiometric hydroxyapatite is usually conveyed as 1.67, while Ca/P ratio of non-stoichiometric calcium deficient hydroxyapatite is below 1.67. Compared to synthetic HAp, natural HAp is non-stoichiometric since it contains trace amounts of Na^+, Zn^{2+}, Mg^{2+}, K^+, Si^{2+}, Ba^{2+}, F^- and CO_3^{2-}. Hydroxyl being the end member of the hydroxyapatite complex is replaceable by carbonate, chloride or fluoride ions. Thus, calcium deficient non-stoichiometric HAps derived from natural sources has shown to be a better adsorbent for the purification of aqueous solutions containing metal cations, anions and organic pollutants due to presence of exchangeable cation, hydroxyl ions and phosphate chelating group [8,

✉ Ilaiyaraja Perumal
ilaiyaraja.perumal@vit.ac.in

1 Chemistry Division, School of Advanced Sciences, Vellore Institute of Technology, Chennai, Tamil Nadu 600127, India

2 Department of Physics, Aarupadai Veedu Institute of Technology, Vinayaka Mission's Research Foundation, Chennai, Tamil Nadu 603 104, India

3 Department of Chemistry, Sri Sivasubramaniya Nadar College of Engineering, Kalavakkam, Tamil Nadu 603110, India

4 Department of Physics, Arunai Engineering College, Tiruvannamalai, Tamil Nadu 606 603, India

5 Department of Physics, Salem Sowdeswari College (Govt. Aided), Salem, Tamilnadu 636 010, India

9]. Currently studies were focused on the use of bio-based sources such as coral, egg shells, fish bones, and seashells for the preparation of HAp. Among the above sources, seashell wastes are considered as the potential materials due to their availability and rich calcium content (> 95wt% $CaCO_3$). Seashell wastes were also utilized in chemical synthesis to produce novel functional materials for environmental remediation applications [10].

The present work aims to use *Perna viridis* sea shell natural bio waste for synthesis of HAp and study its adsorption potential for removal of U(VI) from aqueous medium. U(VI) is a natural radioactive elements present on the earth crust. Development of nuclear energy technology has resulted in the release of U(VI) into the environment both by the front end and back end of nuclear fuel cycle. The formation of various hydrolysed U(VI) species such as $(UO_2)_3(OH)_5^+$, $UO_2(OH)^+$, and $(UO_2)_2(CO_3)_3^{2-}$ [11, 12] in aqueous medium results in easy migration of U(VI) into the aqueous environment. The elevated level of U(VI) in aqueous medium can cause devastating damage to living organisms through bio-magnification [13]. Hence it is highly important to continuously monitor the level of U(VI) and its removal from aqueous environment. The removal of uranium from the environment has been successfully accomplished using a variety of methods and strategies. Chemical precipitation [14], solidification [15], ion exchange [16], photocatalytic degradation/oxidation [17, 18], membrane separation [19], and solid phase extraction [20] are the prominent approaches. Solid phase extraction is perceived to be an economical process for uranium pre-concentration and extraction [19, 21]. For the efficient extraction of U(VI), adsorbents with phosphate functional moieties are preferred due to the presence of hard donor atoms ("O") which can readily form strong complexes with U(VI). Since, HAp has phosphate functional group along with labile calcium and hydroxyl ions it can be employed as a strong sorbent for uranium decontamination from aqueous medium. Few recent studies with HAp and its composite materials have been reported for U(VI) removal. However, the reported HAps were synthesized using calcium chemical precursor [22–30].

The present work discusses the synthesis of HAp from *Perna viridis* sea shell natural bio waste by chemical precipitation method. The amorphous HAp obtained was annealed with addition of PVA polymer to get rod like nanohydroxyapatite (nHAp). PVA polymer addition during annealing could have modified the exterior surface of the HAp nanoparticles thereby improving the stability and mechanical properties of the materials [31]. Thus, the obtained rod like nanohydroxyapatite (nHAp) have been used for removal of U(VI) ions from aqueous medium and the results are discussed in detail.

Materials and methods

Materials

The biowaste (species: *Perna viridis*) were collected from different sites of Vellar Estuary at Parangipet (Lat: 11°20′ 25.55″ N, Long: 79°45′ 38.62″ E), Tamilnadu, India. Detailed sampling information was given in our previous article [32]. The collected shells were first washed with normal water many times later the meat and algae in the shells were removed by soaking them in hot water for 30 min and then cleaned with running water. Finally, the obtained shells were dried in a hot air oven at 100 °C for 3 h. Diammonium hydrogen phosphate ($(NH_4)_2HPO_4$, Nitric acid (HNO_3), Sodium hydroxide (NaOH), Poly vinyl alcohol (PVA, Mw: 115,000), and acetone of analytical grade were purchased from Merck. $UO_2(NO_3)_2{\cdot}6H_2O$ (98%) was purchased from SRL. U(VI) stock solution was prepared by dissolving 211 mg of $UO_2(NO_3)_2{\cdot}6H_2O$ in 100 mL of 0.1 mol L^{-1} HNO_3 solution.

Synthesis of rod-like nanohydroxyapatite (HAp-NR)

The cleaned and dried *Perna viridis* sea shell bio waste were crushed using agate mortar to get powdered $CaCO_3$ and then calcined at 900 °C for 3 h to get CaO. About 2 g of CaO was dissolved by adding 10 mL of concentrated HNO_3 and evaporated to dryness to get $Ca(NO_3)_2$ crystal. The aqueous solution of $Ca(NO_3)_2$ was prepared by adding 50 mL of deionized water into $Ca(NO_3)_2$ crystal. A white milky precipitate was obtained by slowly adding 0.06 M of $(NH_4)_2HPO_4$ to the above solution (pH of the solution maintained at 9). The precipitate was centrifuged for settling and re-dispersed in deioniozed water and again centrifuged. This process is repeated several times to remove any excess NH_4^+ and NO_3^- ions. Finally, the precipitate was allowed for drying at 100 °C for 3 h in a hot air oven. The resultant powder sample obtained was mixed with PVA polymer and calcined in an air atmosphere at 900 °C for 3 h using an electrical furnace. The synthesis procedure is shown in Fig. 1.

Characterization

Infrared spectrum was recorded using KBr discs by Perkin Elmer FTIR spectrometer in the range of 4000–400 cm^{-1} with a resolution of ± 1.0 cm^{-1} in transmittance mode. X-ray diffraction (XRD) patterns of the powdered samples were obtained using an X'pert PRO diffractometer. CuK_α radiation (λ = 1.54060 A˚) source was used to record the samples at room temperature with the range from 20° to 60°. The scanning electron microscopy (SEM) images was acquired

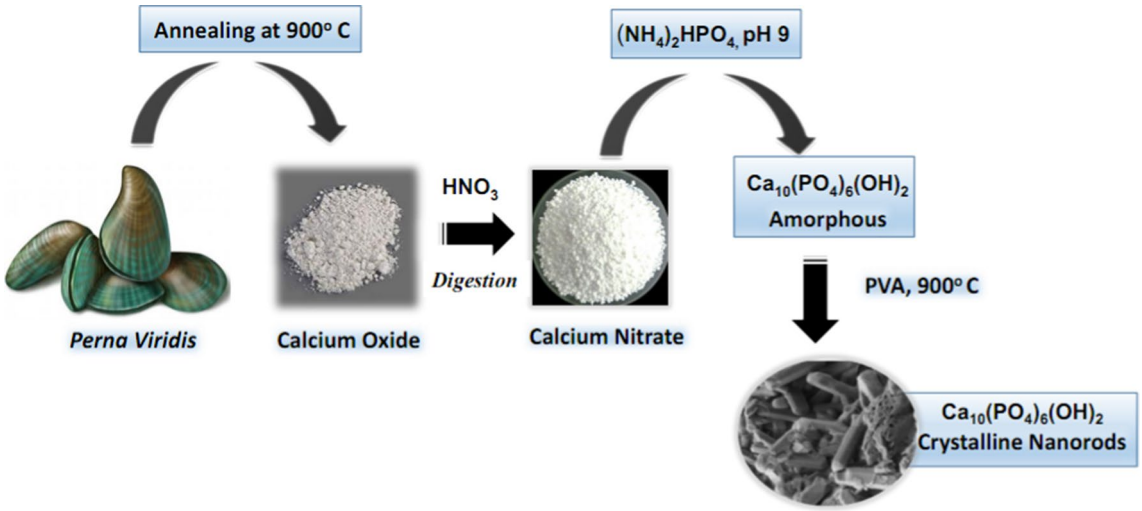

Fig. 1 Scheme of hydroxyapatite Nano-Rod (HAp-NR) synthesis from *Perna* viridis(PV) sea shell bio-waste

using a CARL ZEISS-SIGMA-300 operated at an accelerating voltage of 0.3 to 30 kV, with a resolution of 15 nm (1 kV) at high vacuum mode (HV). Mapping with Energy –Dispersive –X ray (EDX) measurement was carried out using BRUKER at 129 eV. Transmission electron microscope (TEM) images were obtained from Jeol/JEM 2100, Source: LaB6make, Resolution: Point: 0.23 nm.

U(VI) adsorption studies

Application of HAp-NR for the removal of U(VI) from wastewater was studied by batch adsorption technique. All the adsorption experiments were carried out at ambient conditions using a borosilicate glass bottle of 60 ml capacity with a lid under the agitation of 170 rpm. Equilibration of 10 ml of 20 ppm U(VI) solution with 50 mg of HAp-NR was performed to know the adsorption properties of the HAp-NR adsorbent. After three hours of equilibration, phase separation was done by centrifugation. The amount of U(VI) left out in the supernatant after phase separation was estimated using Arsenazo III solution by UV visible spectrophotometric (Perkin Lamda 35 spectrophotometer) method by measuring the absorbance at 655 nm [33].

The amount and percentage of U(VI) adasorbed on HAp-NR are calculated according to the Eqs. (1) and (2).

$$q_e = \frac{(C_o - C_e)}{m} \cdot V \tag{1}$$

$$\%\ \text{Removal} = \frac{(C_o - C_e)}{C_0} \cdot 100 \tag{2}$$

where q_e is the adsorption capacity of HAp-NR in mg g^{-1} of U(VI), C_0 and C_e (mg L^{-1}) are the initial and equilibrium concentration of U(VI) respectively, V (L) is the volume of the solution in litre and m is the weight of the adsorbent (g).

Results and discussion

FTIR studies

Figure 2 shows the FTIR spectra of synthesized HAp-NR at 900 °C. The absorption bands located at 3433 $cm^{-1}(\upsilon_4)$ correspond to the stretching vibration of the hydroxyl groups (OH^-). The band at 961 $cm^{-1}(\upsilon_1)$ is attributed to the symmetric stretching mode of phosphate group. The doublet found at 1091 and 1047 $cm^{-1}(\upsilon_3)$ corresponds to the asymmetric stretching, and a doublet at 605 and 566 $cm^{-1}(\upsilon_4)$ is the bending modes of phosphate group. Presence of the above mentioned characteristics bands indicate that the derived product is HAp. [34, 35].

In addition to the OH^- and PO_4^{3-} peaks, some peaks are observed at 1457 and 876 cm^{-1}. These observed peaks are due to the presence of B type carbonate (CO_3^{2-}) [36] which could be because of the partial replacement of phosphate (PO_4^{3-}) ions by CO_3^{2-} [37].

XRD characterization

Figure 3 shows typical diffraction peaks at 2θ = 25.83°, 28.73°, 31.8°, 32.19°, 32.52°, 34.37°, 39.57°, 41.83°, 46.74°, 47.67°, 49.53°, 53.61° and 64.08° which corresponds to (h k l) of (002), (210), (211), (112), (300), (202), (310), (311), (222), (312), (123), (004) and (304) of the HAp-NR respectively. These diffraction patterns correspond to the hexagonal phase of HAp (a = b ≠ c) with phase group of $P6_3/m$ and unit cell constant a = b = 9.4180 and c = 6.8840 A°, which

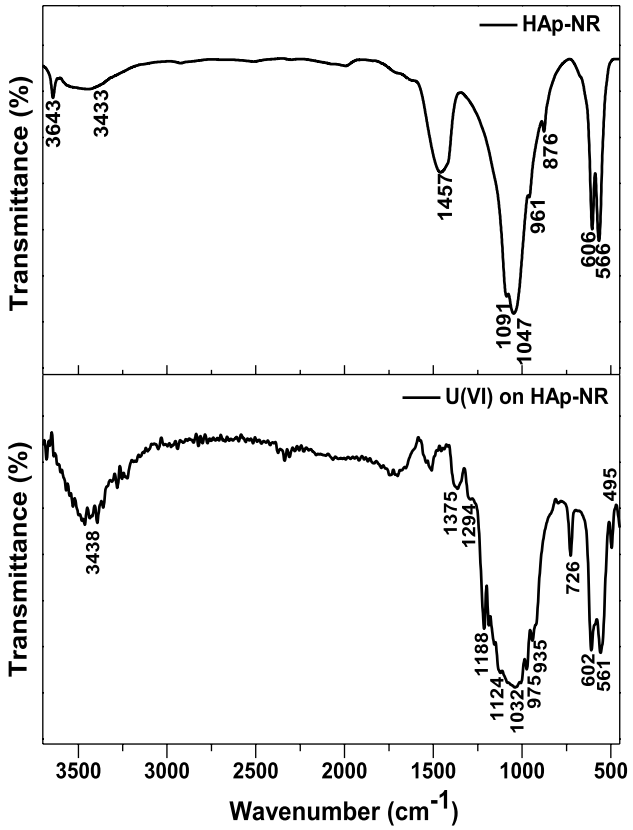

Fig. 2 FTIR spectrum of HAP-NR and U(VI) adsorbed HAp-NR

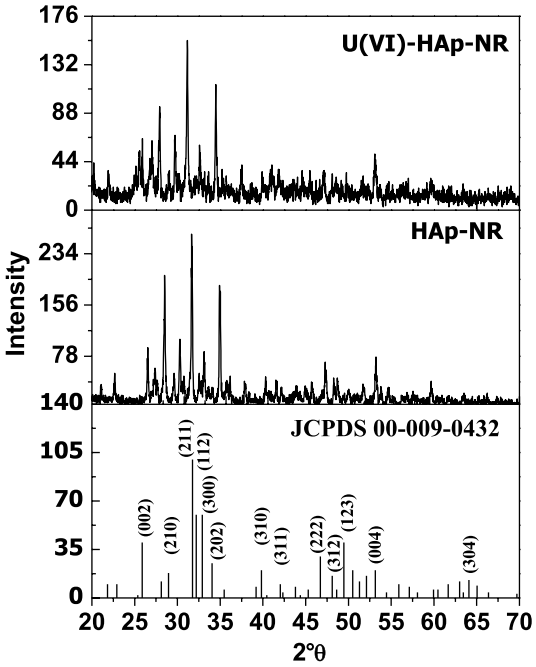

Fig. 3 XRD Pattern of HAp-NR and U(VI) adsorbed HAp-NR

are in well agreement with JCPDS: 09–0432 and previous reports [38–40]. Moreover, there is no additional peak found other than HAp. It is a clear indication that the present XRD patterns solely represent the formation of HAp. The average crystallite size of the synthesized HAp-NR nanoparticles is calculated by Debye- Scherrer's formula as follows (Eq. 3) [41]

$$d = \frac{0.89\lambda}{\beta \mathrm{Cos}\theta} \tag{3}$$

where 'd' is the average crystallite size (in nm), wavelength (λ) = 1.54056 Å for CuK_{α} radiation, β denotes the full width at half maximum (FWHM in radian) of peak and θ is Bragg angle in radian. The average crystallite size of HAp-NR is 41.50 nm. It is important to note that the steric hindrance caused by PVA polymer added during annealing results in a controlled nucleation rate of nanoparticles that decreases the crystallite size [37, 42]

Microstructure analysis of HAp-NR by SEM and TEM

The surface morphology of HAp-NR was analyzed by SEM (Fig. 4a). The morphology of HAp-NR clearly shows a rod like structure. The addition of PVA polymer results in formation of rod-like HAp through nucleation, surface-regulation, growth, oriented attachment and Ostwald ripening mechanism [37, 43, 44]

TEM images and SAED pattern of HAp-NR are shown in Fig. 4b and c. TEM image clearly display rough rod like structure of HAp-NR. SAED pattern indicates the presence of polycrystalline nature of HAp-NR with an inter-planar distance of 0.41 nm (Fig. 4c). Figure 4d shows the EDX spectrum of HAp-NR and it confirms the presence of Ca, P and O elements with Ca/P ratio = 1.61 which is very close to theoretical ratio of 1.67.

Uranium uptake by HAp-NR adsorbent

Effect of pH on U(VI) speciation and its adsorption onto HAp-NR

The synthesized HAp-NR was used as an adsorbent for uptake of uranium from aqueous solutions. U(VI) adsorption onto HAp-NRs is highly influenced by the pH of the solution. Figure 5 depicts the percentage of sorption of U(VI) onto HAp-NR as a function of equilibrium pH. At acidic conditions, i.e., pH below 4, the presence of H^+ ions in the solution significantly compete with UO_2^{2+} species suppressing the sorption of U(VI) onto HAp-NR. Hence, the minimum sorption (< 75%) of U(VI) was observed at acidic pH. The maximum sorption of U(VI) on HAp-NR was found to occur at a pH range of 5–7. U(VI) exists

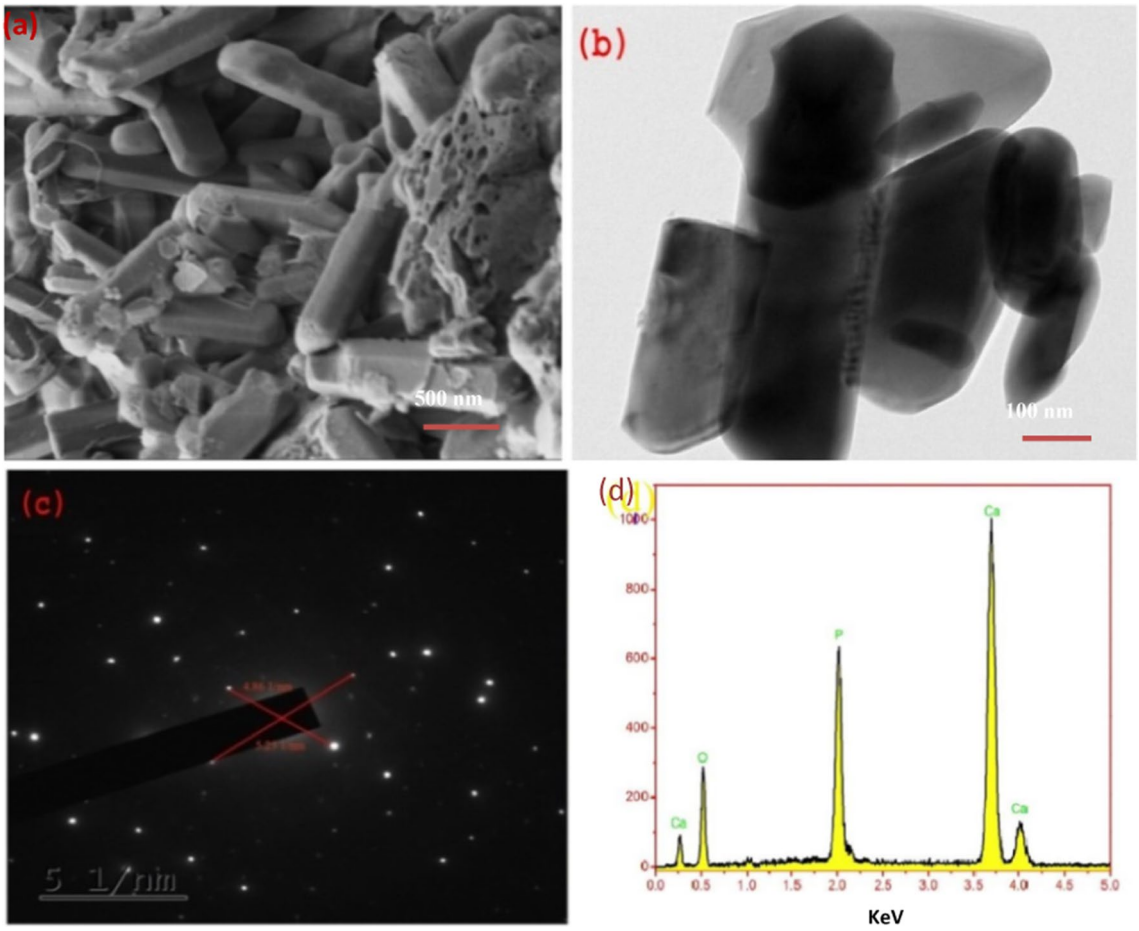

Fig. 4 **a** SEM image, **b** TEM images and, **c** SAD Pattern, **d** EDX spectrum of HAP-NR

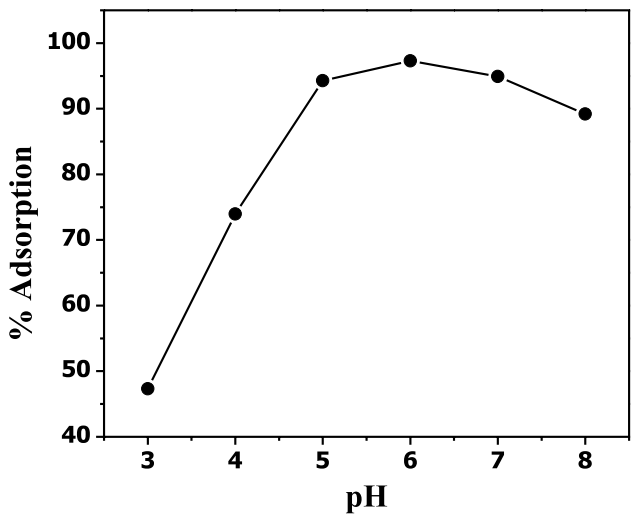

Fig. 5 Effect of pH on uranium adsorption onto HAp-NR

as linear dioxo cation, UO_2^{2+} at pH ≤ 2.5 and it undergo hydrolysis beyond pH 3. An appreciable amount of mononuclear UO_2OH^+ species is present between pH 5 and 7. The decrease in H^+ ion concentrations and favorable interaction of UO_2OH^+ species with HAp-NR resulting in maximum sorption at a pH range of 5–7 [11, 12]. The results show that maximum of ~ 97% of U(VI) adsorbed on HAp-NR at pH 6. The formation of dinuclear species both cationic and anionic dinuclear species such as $(UO_2)_3(OH)_5^+$, $(UO_2)_2(OH)_2^{2+}$, $(UO_2)_4(OH)_7^+$, $(UO_2)_2CO_3(OH)_3^-$, $(UO_2)_3(OH)_7^-$ and $(UO_2)_2(CO_3)_3^{4-}$ increases from pH 6. The electrostatic repulsion of anionic dinuclear U(VI) species with the surface of HAp-NR adsorbent results in decrease of U(VI) sorption onto HAp-NR at pH > 6.

Kinetics of adsorption

The practical application of an adsorbent depends on the kinetics of adsorbate sorption on the adsorbent surface. The kinetics of U(VI) sorption onto the HAp-NR adsorbents were investigated over the period of 1–180 min. Typically,

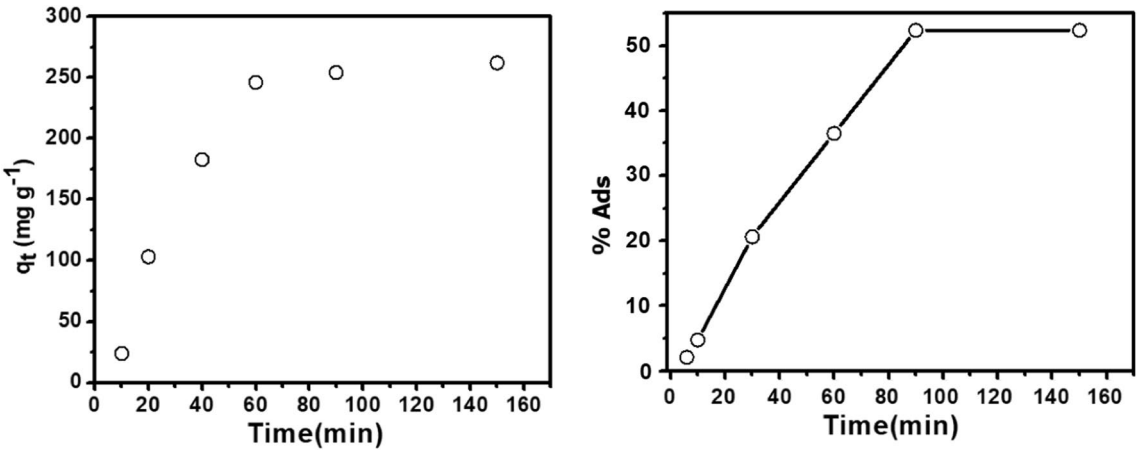

Fig. 6 Kinetics of uranium adsorption on HAp-NR

0.1 g of the adsorbent was dispersed in 25 mL of millipore water and then equilibrated with 25 ml of 100 ppm U(VI) solution which was pre-adjusted to a pH of 6. At periodic time intervals, the concentration of U(VI) in the supernatant of the solution was determined. The kinetics of U(VI) adsorption onto HAp-NR in terms of adsorption capacities (q_t) and percentage of adsorption are shown in the Fig. 6. The kinetics experiment illustrates that the sorption process takes place gradually and then it attains equilibrium within 90 min. After 90 min of equilibration, percentage of U(VI) sorption remains constant due to saturation of active sites of the adsorbent.

Four kinetic models, pseudo-first-order, pseudo-second-order, Elovich and intra-particle diffusion kinetic models were used to fit the experimental data of U(VI) adsorption on the HAp-NR (Fig. 7a–d). The equation of these four kinetics models in the linear form is given in Eqs. (4)–(7), respectively.

$$\text{Pseudo} - \text{first order} \quad \ln\left(q_e - q_t\right) = \ln q_e - k_1 t \tag{4}$$

$$\text{Pseudo - second order} \quad \frac{t}{q_t} = \frac{1}{k_2 q_e^2} + \frac{t}{q_e} \tag{5}$$

$$\text{Elovich} \quad q_t = \frac{1}{\beta}\ln(\alpha\beta) + \frac{1}{\beta}\ln t \tag{6}$$

$$\text{Intra particle diffusion models} \quad q_t = k_i t^{0.5} + c \tag{7}$$

The kinetic parameters and the regression coefficients (R) for above four models of the adsorption process were calculated from the corresponding linear plots and listed in Table 1. The experimental kinetic data has strong correlation with Elovich kinetic model and the value of regression coefficients (R) is better compared to other kinetic models (Table 1). The Elovich kinetic model has been applied satisfactorily to chemisorption data and it is often valid for heterogeneous adsorption systems [45]. The present experimental data suggests that the adsorption of U(VI) onto HAp-NR was controlled by chemisorption. The Elovich kinetic parameters such as initial velocity (α) and desorption constant (β) were estimated by a linear plot of q_t against lnt (Fig. 7c). The parameters α and β calculated from the intercept and the slope of the lines are found to be 14.2 mg/g min and 0.009 g/mg respectively. The moderate velocity and low desorption constant strongly suggest the most favorable sorption of U(VI) onto HAp-NR adsorbent.

Adsorption capacity of HAp-NR

The maximum U(VI) sorption capacity (q_m) of HAp-NR was investigated by equilibrating 0.05 g of HAp-NR with various concentrations of U(VI) between 50 mg L^{-1} and 500 mg L^{-1} for a contact time of 1 h. Figure 8 clearly shows that, the equilibrium adsorption capacity (q_e) increased with increase in initial U(VI) concentration and reached to a maximum value. The experimentally determined maximum sorption capacity (q_m) of HAp-NR was found to be 293.6 mg g^{-1}.

Adsorption isotherms

The initial U(VI) concentration dependent sorption isotherm data were fitted with the linear forms of Langmuir and Freundlich isotherm models (Eqs. 8 and 9). These two models were commonly employed to describe the interaction between the adsorbent and the adsorbate [45].

$$\text{Langmuir} \quad \frac{C_e}{q_e} = \frac{1}{q_{0b}} + \frac{C_e}{q_0} \tag{8}$$

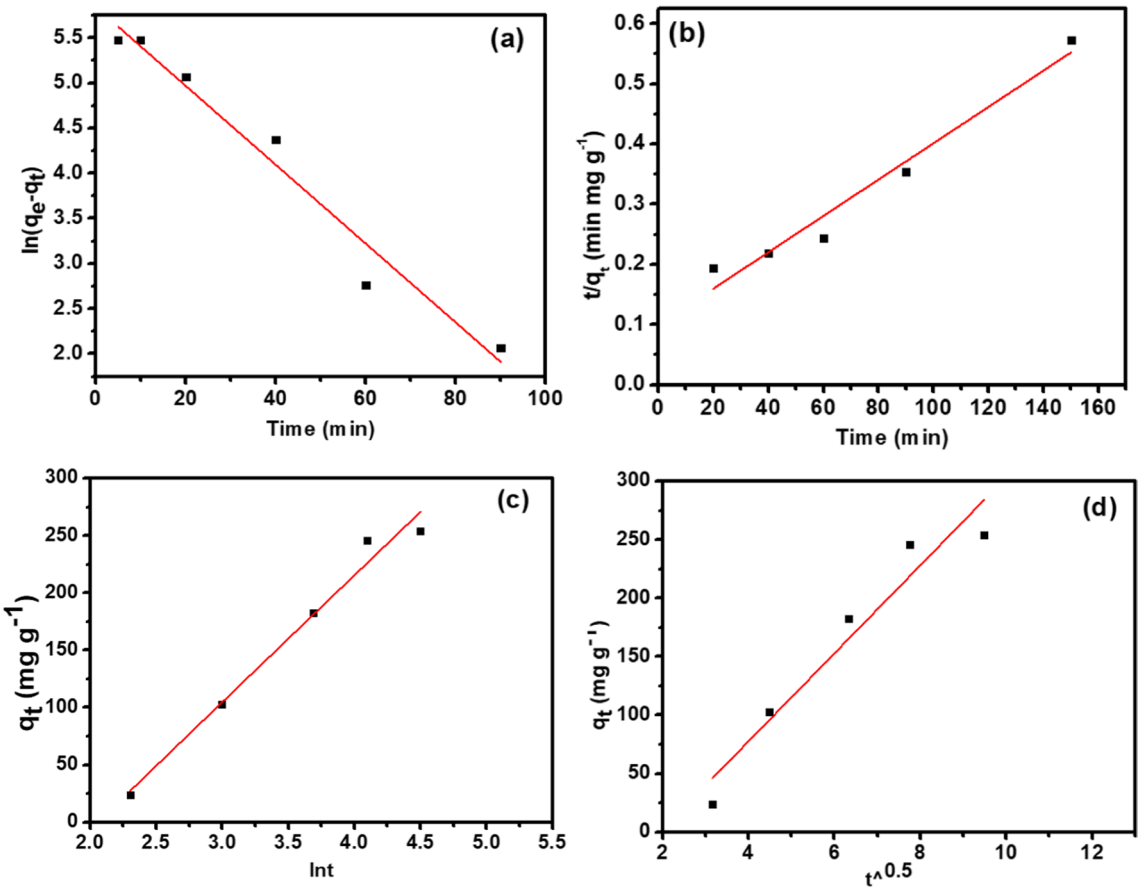

Fig. 7 The linear fit of experimental data of U(VI) adsorption onto HAp-NR according to **a** pseudo-first-order, **b** pseudo-second-order, **c** Elovich and **d** intra-particle kinetic models

Table 1 Kinetic parameters for U(IV) adsorption onto HAp-NR

Kinetic parameters	
Pseudo First Order	
k_1 (min^{-1})	0.0436
q_e (mg g^{-1})	343.7
R^2	0.958
Pseudo Second Order	
K_2 (min^{-1})	0.000103
q_e (mg g^{-1})	312.5
R^2	0.955
Elovich	
α (mg g^{-1} min^{-1})	14.2
β (g mg^{-1})	0.009
R^2	0.975
Intra-particle diffusion	
k_i (mg $g^{-1}min^{1/2}$)	37.62
c (mg g^{-1})	− 72.8
R^2	0.912

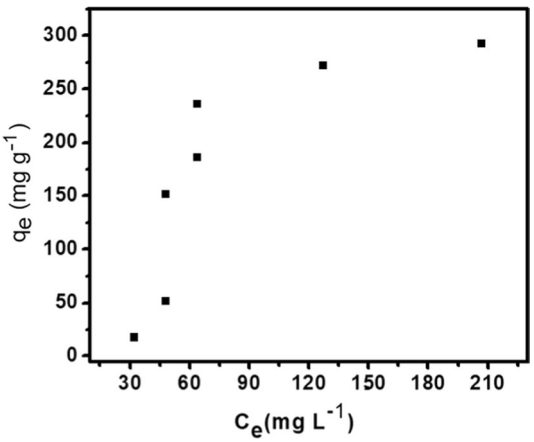

Fig. 8 Effect of initial U(VI) concentration on the sorption capacity of HAp-NR

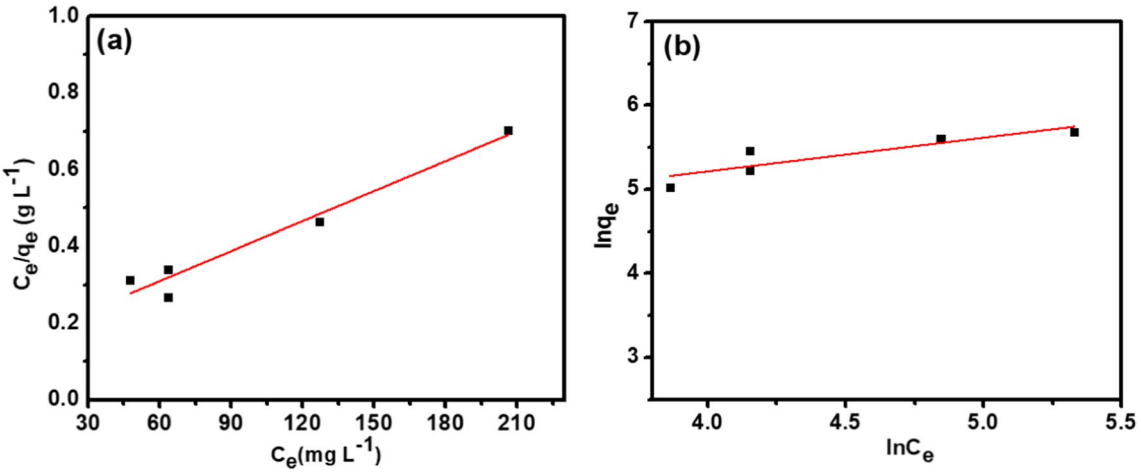

Fig. 9 **a** Langmuir and **b** Freundlich isotherm plot for the removal of U(VI) by HAp-NR (T = 25 °C, pH 6.0, shaking time 180 min, amount of nHAp 0.05 g)

$$\text{Freundlich} \quad \ln q_e = \ln K_F + \frac{1}{n}\ln C_e \tag{9}$$

where q_o (mg g^{-1}) and b (L mg^{-1}) are the Langmuir sorption capacity and energy, respectively. K_F (mg^{1-n} L^n g^{-1}) and n are empirical Freundlich constants which represents the extent of adsorption and the degree of nonlinearity respectively. The Langmuir and Freundlich isotherm fit for U(VI) adsorption onto HAp-NR are shown in Fig. 9a and b and the parameters obtained are given in Table 2. It is observed that Langmuir model fits the sorption data fairly better than the Freundlich model. The above findings illustrates that U(VI) is uniformly adsorbed on the surface of HAp-NR. Therefore, the adsorption process is mainly predominated by chemisorption.

Mechanism of U(VI) adsorption on HAp-NR adsorbent

HAp-NR is composed of $Ca_{10}(PO_4)_6(OH)_2$ and it is expected that the adsorption of U(VI) on HAp-NR mainly occurs via ion exchange of U(VI) species with Ca^{2+} ions and the complexation with phosphate chelating groups [46]. The U(VI) species substitutions in hydroxyapatite lattices is complex, there may be an unequal distribution of U(VI) species in the HAp due to presence of various hydrolysed U(VI) species (UO_2^{2+}, $UO_2(OH)^+$) in the aqueous medium. The charge compensation mechanism plays a significant role during U(VI) species substitution on the Ca^{2+} ions site of HAp-NR. The (VI) species substitution on the Ca^{2+} ions site and complexation with phosphate chelating groups of HAp-NR is shown in Fig. 10. The presence of U(VI) species on the surface of HAp-NR was confirmed by FTIR, XRD and SEM–EDS. FTIR spectrum for U(VI) species adsorbed on HAp-NR adsorbent is shown in Fig. 2. FTIR spectrum shows a significant shift in the vibrational peaks at 1047 cm^{-1} to 1032 cm^{-1} corresponding to –P = O stretching of HAp-NR after adsorption of uranium strongly indicates that phosphate groups are complexing with U(VI) species. In addition to HAp vibrational peaks, the new peaks at 726, 935 and 495 cm^{-1} are observed corresponding to stretching vibrational peaks of O=U=O and U–O respectively [47]. Moreover, a very broad vibrational peak centered at 3438 cm^{-1} clearly indicates the adsorption of hydrolysed $UO_2(OH)^+$ species on the surface of HAp-NR adsorbent. XRD pattern of U(VI) adsorbed HAp-NR reveals that there is no additional peak found other than HAp however a significant decrease in peak intensity of diffraction pattern and increased background in the XRD spectrum (Fig. 3) indicates surface modification in HAp-NR adsorbent [47]. That is adsorption of U(VI) species on the surface of HAp-NR leads to observable changes in the XRD spectrum of U(VI)-HAp-NR. The adsorption of U(VI) species and resultant surface modification of HAp-NR was also confirmed by SEM–EDS analysis. The surface of the HAp-NR rods was relatively smooth with abundant pore structures before adsorption (Fig. 5). After U(VI) adsorption (Fig. 11), the HAp-NR rods surface

Table 2 Adsorption Isotherm parameters for U(VI) adsorption on HAp-NR

Isotherm Parameters	Values
Langmuir	
q_o (mg g^{-1})	384.6
B	0.017
R^2	0.948
Freundlich	
K_F (mg g^{-1})	037.0
n	2.495
R^2	0.713

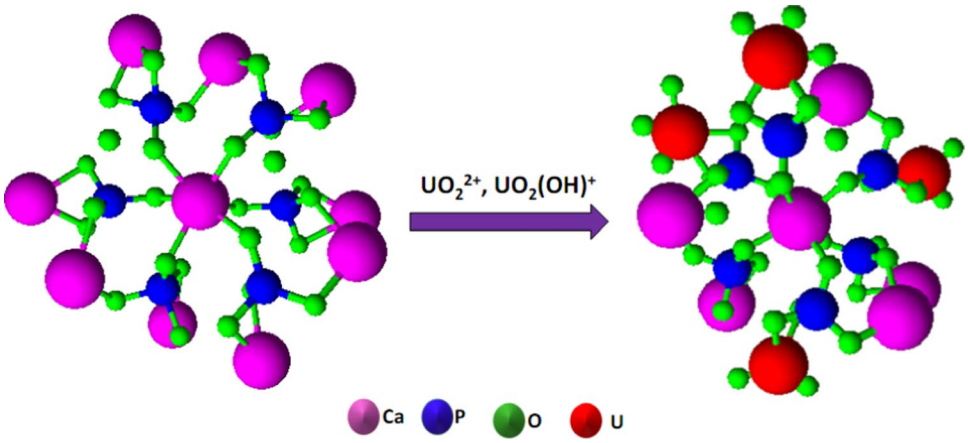

Fig. 10 Sorption of U(VI) onto HAp-NR by ion-exchange and chelation

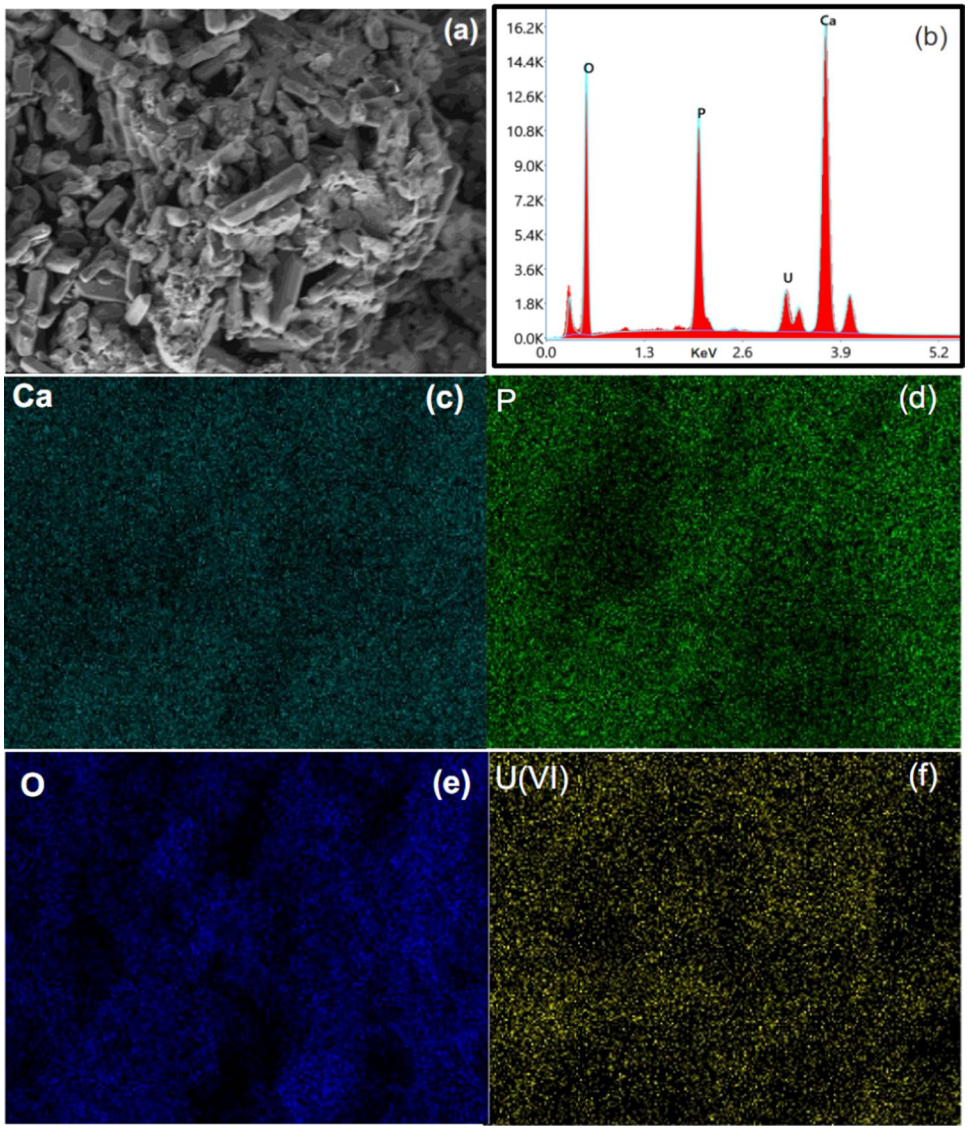

Fig. 11 **a** SEM, **b** EDS elemental analysis and Elemental mappings for **c** Ca, **d** P, **e** O, and **f** U(VI) from the U(VI) adsorbed HAp-NR adsorbent

became relatively rough along with the appearance of irregular large particles. The changes observed before and after U(VI) adsorption serves as a strong evidence that U(VI) species have occupied the active sites and also entered the pores on the surface of HAp-NR (Fig. 11f). The elemental analysis reveals that about 7.3% weight and 0.68 atomic percentage of U(VI) adsorbed onto HAp-NR (Table 3). Hence, FTIR, XRD and SED-EDS studies strongly supports the adsorption of U(VI) species onto HAp-NR.

Comparison of adsorption capacity of HAp-NR with other relevant reported adsorbent

The experimental maximum sorption capacities of various hydroxyapatite materials and its composites for U(VI) uptake are given in Table 4 [21–30]. The comparative results on the adsorption capacities would provide useful insights on the criterion for the assessment of the adsorbents for practical applications. The table clearly shows that the sorption capacity of rod-like nanohydroxyapatite (HAp-NR) from *perna viridis (pv)* bio-waste shell in the present study is reasonable, and it is high compared to many other reported adsorbents.

Thermodynamics study

The determination of thermodynamic parameters is very important to know about the spontaneity of a chemical process. Thermodynamic parameters such as Gibb's free energy (ΔG), enthalpy (ΔH) and entropy (ΔS) were obtained by carrying out adsorption at different temperatures (30 °C to 80 °C). Enthalpy (ΔH) and entropy (ΔS) were obtained from slope and intercept of the linear plot of $\ln K_d$ versus 1/T using Van't Hoff Eq. (10) and ΔG was calculated using standard thermodynamic Eq. (11). The linear plot of $\ln K_d$ versus 1/T is shown in Fig. 12 and calculated thermodynamic parameters are summarized in Table 5.

$$\ln K_d = \frac{\Delta S^o}{R} - \frac{\Delta H^o}{RT} \tag{10}$$

$$\Delta G^o = \Delta H^o - T(\Delta S^o) \tag{11}$$

where R (8.314 J/mol/K) is the ideal gas constant and T (K) is the temperature in Kelvin.

Table 3 Elemental analysis of HAp-NR after U(VI) adsorption

Element	Weight (%)	Atom (%)	Error (%)
O K	55.90	77.38	10.40
P K	09.87	07.06	04.65
Ca K	26.93	14.88	02.64
U M	07.30	0.68	04.44

Table 4 Comparison of experimental U(VI) maximum sorption capacity of HAp-NR with various adsorbents

Adsorbent	Sorption capacity ($mg\ g^{-1}$)	References
HAp-AC-Alginate	18.66	[21]
Porous HAp	111.4	[22]
Carbonated hydroxyapatite	123.8	[23]
HAp microspheres	199	[24]
Al-doped Hap (Al-HAp-5)	222.2	[25]
Magnetically modified hydroxyapatite	310	[26]
HAp@kaolin aerogel	401.6	[27]
HAp-modified ZIF-67 composite	453.1	[28]
Mg/Fe-LDHs@nHAp nanoscale materials	545	[29]
HAp (Microbial synthesis)	1025	[30]
Bio-waste derived HAp NanoRod	293.6	This work

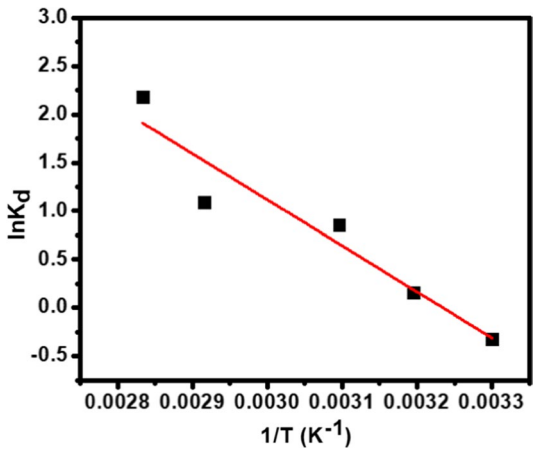

Fig. 12 Effect of temperature on U(VI) adsorption onto HAp-NR

The positive value of ΔH° reveals the endothermic nature of the adsorption process and positive value of ΔS refers to the increase in randomness during adsorption process. Entropy's positive value suggest that entropy increase due to the de-solvation of adsorbate species overcome the decrease in entropy due to attachment of adsorbate species an adsorbent surface which results in overall entropy increase for adsorption process. Adsorption of U(VI) species involves desolvation of hydration sphere and then adsorption on the surface of HAp-NR. The desolvation is an endothermic process and thus the increase in solution temperature favours the adsorption process. Hence, the Gibb's free energy change (ΔG) is negative at temperature > 313 K which indicates the adsorption is more favourable above 313 K.

Effect of ionic strength on U(VI) adsorption

Ionic strength that is concentration of Ca^{2+}, Na^{+}, K^{+}, Cl^{-}, NO_3^{-} and CO_3^{2-} drastically vary depending on the nature of surface waters and environment. Hence, we studied the influence of ionic strength of aqueous solution on U(VI) uptake onto HAp-NR. A stock solution consisting of 1 M concentration was prepared by weighing required amount of $CaCl_2$, NaCl and KCl salts and together dissolved in 100 mL of deionized water. In the total 10 ml of aqueous solution, 25 mg of HAp-NR, 50 ppm of U(VI) were kept constant and varied the electrolyte concentration from 0.001 M to 0.1 M. Figure 13 shows, as the ionic strength of aqueous solution increased, U(VI) uptake on HAp-NR decreases gradually. The percentage of U(VI) adsorption on HAp-NR from aqueous solution of ionic strength of 0.01 M is about 87%. However, the concentrations of ions in natural waters are far below than 0.01 M [48]. Hence, HAp-NR can be adopted as a potential adsorbent for U (VI) adsorption from surface waters.

Reusability of HAp-NR adsorbent

To check the reusability of HAp-NR adsorbent, desorption of U(VI) species was performed by equilibrating separately with 10 ml of 0.001 M to 0.25 M concentration of hydrochloric acid (HCl) and sodium carbonate (Na_2CO_3) solutions [49]. Figure 14 shows more than 85% and 92% of the adsorbed U(VI) species were desorbed using 0.05 M HCl and Na_2CO_3 respectively. Further increase in the concentration of HCl and and Na_2CO_3, increased the percentage of U(VI) desorption. However, the increasing concentration of HCl beyond 0.1 M leads to complete dispersion of HAp-NR nanoparticles in the aqueous solution. Those dispersed HAp-NR nanoparticle were not completely settling during centrifugation even at 6000 rpm. The micro sized HAp-NR might have broken into smaller nanoparticles leading to dispersion in the aqueous solution. While using Na_2CO_3 as desorbing agent HAp-NR nanoparticles were stable and observed better separation of HAp-NR from aqueous solution. Thus, the results reveals that desorption of U(VI) should be carried out using 0.05 M Na_2CO_3, so that HAp-NR adsorbent can be used several times.

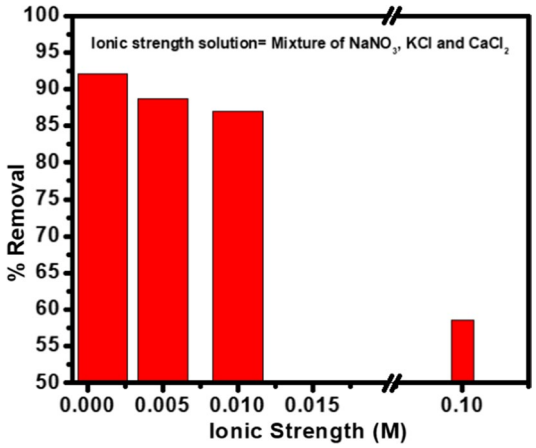

Fig. 13 Effect of ionic strength on U(VI) adsorption onto HAp-NR

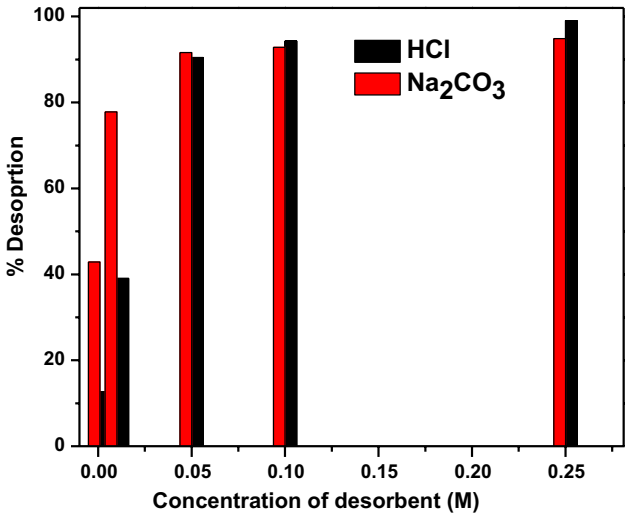

Fig. 14 Desorption of U(VI) from HAp-NR adsorbent

Conclusion

In summary, we synthesized HAp-NR from sea shell bio source (*Perna viridis*) by simple precipitation method. Removal of U(VI) from aqueous solution using biowaste-derived HAp-NR was carried out. The study reveals that HAp-NR is a more suitable material for the remediation of uranyl ions (UO_2^{2+}) from wastewater due to it exceptional sorption capacity (293.6 mg g^{-1}) and adsorption kinetics (equilibrium reached less than 90 min). The uniform

Table 5 Thermodynamic parameters of U(VI) adsorption onto HAp-NR

ΔH^o (kJ mol^{-1})	ΔS^o (kJ mol^{-1})	ΔG^o (kJ mol^{-1})				
		303 K	313 K	323 K	343 K	353 K
39.54	0.127	1.055	− 0.211	− 1.481	− 4.021	− 5.291

adsorption of U(VI) onto HAp-NR adsorbent was clearly observed in SEM–EDX. The exchangeable Ca^{2+} cations and strong coordinating phosphate functional group present in HAp helps in effective adsorption of U(VI) species from aqueous medium. The uranyl ions were adsorbed on HAp-NR via ion exchange and surface complexation mechanism. The U(VI) adsorption further increases with increase in temperature. In addition, HAp-NR can be used to treat surface waters containing U(VI) species in presence of various other ions. Moreover, HAp-NR can be reusable by treating with dil. Na_2CO_3 solution. Thus, the present study clearly depicts that HAp-NR could be an efficient nanomaterial for environmental remediation.

Acknowledgements The authors sincerely thank school of advanced sciences, Vellore Institute of Technology Chennai for providing necessary infrastructure and characterization techniques to carry out this work.

Funding All authors declare that no funds, grants, or other support were received during the preparation of this manuscript.

Declarations

Conflict of interest All authors declare that no conflicts of interest for this research manuscript.

References

1. Kim SK, Venkatesan J (2015) Introduction to marine biotechnology. In: Kim SK (ed) Springer handbook of marine biotechnology. Springer handbooks. Springer, Berlin. https://doi.org/10.1007/978-3-642-53971-8_1
2. Ibrahim A-R, Wei W, Zhang D, Wang H, Li J (2013) Conversion of waste eggshells to mesoporous hydroxyapatite nanoparticles with high surface area. Mater Lett 110:195–197. https://doi.org/10.1016/j.matlet.2013.08.014
3. Ducheyne P, Hench LL, Kagan A, Martens M, Bursens A, Mulier JC (1980) Effect of hydroxyapatite impregnation on skeletal bonding of porous coated implants. J Biomed Mater Res 14:225–237. https://doi.org/10.1002/jbm.820140305
4. Patel N, Brooks RA, Clarke MT, Lee PMT, Rushton N, Gibson IR, Best SM, Bonfield W (2005) In vivo assessment of hydroxyapatite and silicate-substituted hydroxyapatite granules using an ovine defect model. J Mater Sci - Mater Med 16:429–440. https://doi.org/10.1007/s10856-005-6983-6
5. Takikawa K, Akao M (1996) Fabrication of transparent hydroxyapatite and application to bone marrow derived cell/hydroxyapatite interaction observation in-vivo. J Mater Sci Mater Med 7:439–445. https://doi.org/10.1007/BF00122014
6. Ripamonti U, Crooks J, Khoali L, Roden L (2009) The induction of bone formation by coral-derived calcium carbonate/hydroxyapatite constructs. Biomaterials 30:1428–1439. https://doi.org/10.1016/j.biomaterials.2008.10.065
7. Ohare P, Meenan BJ, Burke GA, Byrne G, Dowling D, Hunt JA (2010) Biological responses to hydroxyapatite surfaces deposited via a co-incident microblasting technique". Biomaterials 31:515–522. https://doi.org/10.1016/j.biomaterials.2009.09.067
8. Huber F-X, Berger I, McArthur N, Huber C, Kock H-P, Hillmeier J, Meeder P (2008) Evaluation of a novel nanocrystalline hydroxyapatite paste and a solid hydroxyapatite ceramic for the treatment of critical size bone defects (CSD) in rabbits. J Mater Sci Mater Med 19:33–38. https://doi.org/10.1007/s10856-007-3039-0
9. Neelakandeswari N, Sangami G, Dharmaraj N (2011) Preparation and characterization of nanostructured hydroxyapatite using a biomaterial. Synth React Inorg Met-Org Nano-Met Chem 41(5):513–516. https://doi.org/10.1080/15533174.2011.568434
10. Karunakaran G, Cho E-B, Kumar GS, Kolesnikov E, Janarthanan G, Pillai MM, Rajendran S, Boobalan S, Gorshenkov MV, Kuznetsov D (2019) Ascorbic acid-assisted microwave synthesis of mesoporous Ag-doped hydroxyapatite nanorods from biowaste seashells for implant applications. ACS Appl Bio Mater 2:2280–2293. https://doi.org/10.1021/acsabm.9b00239
11. Priyadarshini N, Sampath M, Kumar S, Mudali UK, Natarajan R (2013) A combined spectroscopic and light scattering study of hydrolysis of uranium(VI) leading to colloid formation in aqueous solutions. J Radioanal Nucl Chem 298:1923–1931. https://doi.org/10.1007/s10967-013-2624-6
12. Priyadarshini N, Benadict Rakesh K, Ilaiyaraja P (2018) Actinide separation in environment and their separation using functionalized nanomaterials and nanocomposits. In: Hussain CM (ed) Handbook of environmental materials management. Springer, Berlin, pp 19–20. https://doi.org/10.1007/978-3-319-58538-3-143-1
13. Rayno DR (1983) Estimated dose to man from Uranium milling via the beef/milk food-chain pathway. Sci Total Environ 31:219–241. https://doi.org/10.1016/0048-9697(83)90078-5
14. Kukkonen E, Virtanen EJ, Moilanen JO (2022) α-Aminophosphonates, phosphinates, and phosphine oxides as extraction and precipitation agents for rare earth metals, thorium, and uranium: a review. Molecules 27:3465. https://doi.org/10.3390/molecules27113465
15. Li S, Hu Y, Shen Z (2021) Rapid and selective uranium extraction from aqueous solution under visible light in the absence of solid photocatalyst. Sci China Chem 64:1323–1331. https://doi.org/10.1007/s11426-021-9987-1
16. Chen F, Lv M, Ye Y, Miao S, Tang X, Liu Y, Liang B, Qin Z, Chen Y, He Z, Wang Y (2022) Insights on uranium removal by ion exchange columns: the deactivation mechanisms, and an overlooked biological pathway. Chem Eng J 434:134708. https://doi.org/10.1016/j.cej.2022.134708
17. Chen T, Zhang J, Ge H, Li M, Li Y, Liu B, Duan T, He R, Zhu W (2020) Efficient extraction of uranium in organics-containing wastewater over g-C_3N_4/GO hybrid nanosheets with type-II band structure. J Hazard Mater 384:121383. https://doi.org/10.1016/j.jhazmat.2019.121383
18. Chen T, Yu K, Dong C, Yuan X, Gong X, Lian J, Cao X, Li M, Zhou L, Hu B, He R, Zhu W, Wang X (2022) Advanced photocatalysts for uranium extraction: elaborate design and future perspectives. Coord Chem Rev 467:214615. https://doi.org/10.1016/j.ccr.2022.214615
19. Yang L, Xiao H, Qian Y et al (2022) Bioinspired hierarchical porous membrane for efficient uranium extraction from seawater. Nat Sustain 5:71–80. https://doi.org/10.1038/s41893-021-00792-6
20. Yuan D, Zhao J, Zhang Q, Peng Lu, Wang Y, He Y, Liu Z, Liu Y, Zhao X, Meng C (2022) Highly efficient extraction of uranium from aqueous solution using imidazole functionalized core–shell sunflower-like superparamagnetic polymer microspheres: understanding adsorption and binding mechanisms. J Mater Chem A 10:12656–12668. https://doi.org/10.1039/D2TA02669D
21. Sahaa S, Basu H, Rout S, Pimple MV, Singhal RK (2020) Nano-hydroxyapatite coated activated carbon impregnated alginate: a new hybrid sorbent for uranium removal from potable water. J Environ Chem Eng 8:103999. https://doi.org/10.1016/j.jece.2020.103999
22. Su M, Tsang DCW, Ren X, Shi Q, Tang J, Zhang H, Kong L, Hou L, Song G, Chen D (2019) Removal of U(VI) from nuclear mining

effluent by porous hydroxyapatite: evaluation on characteristics, mechanisms and performance. Environ Pollut 254:112891. https://doi.org/10.1016/j.envpol.2019.07.059
23. Yanhong Wu, Chen D, Kong L, Tsang DCW, Minhua Su (2019) Rapid and effective removal of uranium (VI) from aqueous solution by facile synthesized hierarchical hollow hydroxyapatite microspheres. J Hazard Mater 371:397–405. https://doi.org/10.1016/j.jhazmat.2019.02.110
24. Han T, Chen W, Cai Y, Lv Z, Zhang Y, Tan X (2022) Immobilization of uranium during the deposition of carbonated hydroxyapatite. J Taiwan Inst Chem Eng 134:104331. https://doi.org/10.1016/j.jtice.2022.104331
25. Zhou H, Xie Y, Wang X, Yang H, Wang Y, Zhang Y (2022) Efficient removal of uraniumin aqueous solution by Al-doped hydroxyapatite: static/dynamic adsorption behaviors and mechanism study. Environ Technol Innov 25:102103. https://doi.org/10.1016/j.eti.2021.102103
26. El-Maghrabi HH, Younes AA, Salem AR, Rabie K, El-Shereafy E-S (2019) Magnetically modified hydroxyapatite nanoparticles for the removal of uranium (VI): Preparation, characterization and adsorption optimization. J Hazard Mater 378:120703. https://doi.org/10.1016/j.jhazmat.2019.05.096
27. Xiong T, Jia L, Li Q, Zhang Y, Zhu W (2022) Efficient removal of uranium by hydroxyapatite modified kaolin aerogel. Sep Purif Technol 299:121776. https://doi.org/10.1016/j.seppur.2022.121776
28. Tang M, Shen J, Xia X, Jin B, Chen K, Zeng T (2022) A novel microbial induced synthesis of hydroxyapatite with highly efficient adsorption of uranyl(VI). Colloids Surf A Physicochem Eng Asp 635:128046. https://doi.org/10.1016/j.colsurfa.2021.128046
29. Xuan K, Wang J, Gong Z, Wang X, Li J, Guo Y, Sun Z (2022) Hydroxyapatite modified ZIF-67 composite with abundant binding groups for the highly efficient and selective elimination of uranium (VI) from wastewater. J Hazard Mater 426:127834. https://doi.org/10.1016/j.jhazmat.2021.127834
30. Guo Y, Gong Z, Li C, Gao B, Li P, Wang X, Zhang B, Li X (2020) Efficient removal of uranium (VI) by 3D hierarchical Mg/Fe-LDH supported nanoscale hydroxyapatite: a synthetic experimental and mechanism studies. Chem Eng J 392:123682. https://doi.org/10.1016/j.cej.2019.123682
31. Suresh Kumar C, Dhanaraj K, Vimalathithan RM, Ilaiyaraja P, Suresh G (2021) Structural, morphological and anti-bacterial analysis of nanohydroxyapatite derived from biogenic (SHELL) and chemical source: formation of apatite. Iran J Mater Sci Eng 18:91–109. https://doi.org/10.22068/ijmse.18.1.10
32. Dhanaraj K, Suresh G (2018) Conversion of waste sea shell (*Anadara granosa*) into valuable nanohydroxyapatite (nHAp) for biomedical applications. Vaccum 152:222–230. https://doi.org/10.1016/j.vacuum.2018.03.021
33. Savvin S (1961) Analytical use of arsenazo III Determination of thorium zirconium, uranium and rare earth elements. Talanta 8:673–685. https://doi.org/10.1016/0039-9140(61)80164-1
34. Sadar SM, Khorasani MT, Dinpanah-Khoshdargi E, Jamshidi A (2013) Synthesis methods for nanosized hydroxyapatite with diverse structures. Acta Biomater 9:7591–7662. https://doi.org/10.1016/j.actbio.2013.04.012
35. Dauphin Y, Denis A (2000) Structure and composition of the aragonite crossed lamellar layers in six species of Bivalvia and Gastropoda. Comp Biochem Physiol Part A 126:367–377. https://doi.org/10.1016/s1095-6433(00)00213-0
36. Nunez D, Elgueta E, Varaprasad K, Oyarzun P (2018) Hydroxyapatite nanocrystals synthesized from calcium rich biowastes. Mater Lett 230:64–68. https://doi.org/10.1016/j.matlet.2018.07.077
37. Suresh Kumar C, Dhanaraj K, Vimalathithan RM, Ilaiyaraja P, Suresh G (2020) Hydroxyapatite for bone related applications derived from sea shell waste by simple precipitation method. J Asian Ceram Soc 8(2):416–429. https://doi.org/10.1080/21870764.2020.1749373
38. Dhanaraj K, Suresh Kumar C, Socrates SH, Vinoth Arulraj J, Suresh G (2021) A comparative analysis of microwave assisted natural (*Murex virgineus* shell) and chemical nanohydroxyapatite: structural, morphological and biological studies. J Aust Ceram Soc 57:173–183. https://doi.org/10.1007/s41779-020-00522-9
39. Suresh Kumar G, Girija EK, Venkatesh M, Karunakaran G, Evgeny Kolesnikov E, Kuznetsov D (2017) One step method to synthesize flower-like hydroxyapatite architecture using mussel shell bio-waste as a calcium source. Ceram Int 43(3):3457–3461. https://doi.org/10.1016/j.ceramint.2016.11.163
40. Bensalah H, Bekheet MF, Younssi SA, Ouammou M, Gurlo A (2018) Hydrothermal synthesis of nanocrystalline hydroxyapatite from phosphogypsum waste. J Environ Chem Eng 6:1347–1352. https://doi.org/10.1016/j.jece.2018.01.052
41. Shanmugam N, Dhanaraj K, Viruthagiri G, Balamurugan K, Deivam K (2016) Synthesis and characterization of surfactant, assisted Mn^{2+} doped ZnO nanocrystals. Arab J Chem 9:S758–S764. https://doi.org/10.1016/j.arabjc.2011.08.016
42. Guan Y, Cao W, Wang X, Marchetti A, Tu Y (2018) Hydroxyapatite nano-rods for the fast removal of Congo red dye from aqueous solution. Mater Res Express 5:065053. https://doi.org/10.1088/2053-1591/aaccb8
43. Sadat-Shojai M, Khorasani MT, Dinpanah-Khoshdargi E, Jamshidi A (2013) Synthesis methods for nanosized hydroxyapatite with diverse structures. Acta Biomater 9:7591–7621. https://doi.org/10.1016/j.actbio.2013.04.012
44. Mehta D, Mondal P, Saharan VK, George S (2017) Synthesis of Hydroxyapatite Nanorods for application in water defluoridation and optimization of process variables: advantage of ultrasonication with precipitation method over conventional method. Ultrason Sonochem 37:56–70. https://doi.org/10.1016/j.ultsonch.2016.12.035
45. Dotto GL, Pinto LAA (2011) Adsorption of food dyes onto chitosan: optimization process and kinetic. Carbohyd Polym 84:231–238. https://doi.org/10.1016/j.carbpol.2010.11.028
46. He Y, Wang Y, Cai C et al (2023) Cotton stalk derived carbon pretreated by microbial fermentation for selective uranium extraction. J Radioanal Nucl Chem. https://doi.org/10.1007/s10967-023-08827-2
47. Sakr AK, Abdel Aal MM, Abd El-Rahem KA, Allam EM, Abdel Dayem SM, Elshehy EA, Hanfi MY, Alqahtani MS, Cheira MF (2022) Characteristic aspects of uranium(VI) adsorption utilizing nano-silica/chitosan from wastewater solution. Nanomaterials 12:3866. https://doi.org/10.3390/nano12213866
48. Liao J, Xiong T, Ding L, Xie Y, Zhang Y, Zhu W (2022) Design of a renewable hydroxyapatite-biocarbon composite for the removal of uranium(VI) with high-efficiency adsorption performance. Biochar 4:29. https://doi.org/10.1007/s42773-022-00154-1
49. Ilaiyaraja P, Singha Deb AK, Ponraju D, Musharaf Ali SK, Venkatraman B (2017) Surface engineering of PAMAM-SDB chelating resin with diglycolamic acid (DGA) functional group for efficient sorption of U(VI) and Th(IV) from aqueous medium. J Hazard Mater 328:1–11. https://doi.org/10.1016/j.jhazmat.2017.01.001

Publisher's Note Springer Nature remains neutral with regard to jurisdictional claims in published maps and institutional affiliations.

Springer Nature or its licensor (e.g. a society or other partner) holds exclusive rights to this article under a publishing agreement with the author(s) or other rightsholder(s); author self-archiving of the accepted manuscript version of this article is solely governed by the terms of such publishing agreement and applicable law.